Pis'ma v ZhETF, vol. 103, iss. 10, pp. 715 – 719 © 2016 May 25

The ferromagnetic origin of Na and Mn co-doped $CaZn_2As_2$ diluted magnetic semiconductor: a first-principles study

L. Hua[1)], *J. N. Zhu, Z. T. Lu*

Nanjing Normal University Taizhou College, 225300 Taizhou, People's Republic of China

Submitted 5 April 2016

We have investigated the electronic structure and magnetic properties of Na and Mn co-doped $CaZn_2As_2$ using density functional theory within the generalized gradient approximation (GGA)+U schemes. We have shown that the ground state magnetic structure of Mn-doped $CaZn_2As_2$ is antiferromagnetic while hole-mediated Zener's p-d exchange is responsible for the origin of ferromagnetism of Na and Mn co-doped $CaZn_2As_2$.

DOI: 10.7868/S0370274X16100052

1. Introduction. Diluted magnetic semiconductors (DMSs) have received much attention due to the possibility of utilizing both charge and spin degrees of freedom in electronic devices [1–3]. In order to realize functional spintronics devices, it is important to have a full control of the carrier density and ferromagnetic Curie temperature (T_c). Prototypical DMS systems such as $Ga_{1-x}Mn_xAs$ and $In_{1-x}Mn_xAs$, however, show severely limited chemical solubility due to the substitution of divalent Mn atoms for the trivalent Ga or In sites. Besides, the simultaneous doping of charge and spin induced by Mn substitution prevents us from optimizing the charge and spin densities independently.

A new type of ferromagnetic DMS that overcomes these difficulties has been discovered recently. Bulk specimens of Li(Zn, Mn)As were successfully fabricated [4], using excess Li concentrations introduced into hole carriers, while independently making the isovalent substitution of Mn^{2+} for Zn^{2+} to achieve local spin doping. Shortly after, Li(Zn, Mn)P with $T_c \sim 40$ K were also fabricated by doping Mn into the I-II-V direct gap semiconductors LiZnP [5]. LiZnPn (Pn = P, As) can be viewed as a derivative of the third family of Fe-based superconductors LiFeAs. Accordingly, the first family of Fe-based superconductor is 1111-type oxypnictides $LaFeAs(O_{1-x}F_x)$. With identical two dimensional crystal structure, three 1111 type DMS systems, (La, Ba)(Zn, Mn)AsO with $T_c \sim 40$ K [6], (La, Ca)(Zn, Mn)SbO with $T_c \sim 40$ K [7], (La, Sr)(Cu, Mn)SO with $T_c \sim 210$ K [8] have been reported. Similarly, bulk form DMS systems of $(Ba,K)(Zn,Mn)_2As_2$ [9, 10] with $T_c \sim 180$ K have been reported. These systems are structurally identical to that of 122 type iron pnictides superconductor $(Ba,K)Fe_2As_2$ with tetragonal $ThCr_2Si_2$ structure. The fourth family of Fe-based superconductors is 11 type $FeSe_{1+\delta}$, which can be paralleled to the well investigated II-VI DMS, i.e., (Zn, Mn)Se. Very recently, bulk specimens of DMS $(Ca,Na)(Zn,Mn)_2As_2$ [11] and $(Sr,Na)(Zn,Mn)_2As_2$ [12] with the hexagonal $CaAl_2Si_2$ structure have been reported. In this paper, we have performed a first-principles density functional theory study on $(Ca,Na)(Zn,Mn)_2As_2$ and discussed its ferromagnetic origin.

2. Computational method. The first-principles calculations were performed by using density functional theory (DFT) method within the Perdew-Burke-Ernzerhof (PBE) generalized gradient approximation (GGA) [13], implemented in the Vienna *ab initio* Simulation Package (VASP) [14]. The strong-correlated correction was considered with GGA+U method [15] to deal with the Mn's 3d electrons. The effective onsite Coulomb interaction parameter (U) and exchange interaction parameter (J) are set to be 4.0 and 1.0 eV for Mn's 3d electrons. These values have been tested and used in the previous experimental and theoretical works [16, 17]. For Zn atoms, the strong-correlated correction was not applied as their 3d orbitals are fully occupied. 3p4s for Ca, 3d4s for Zn, 4s4p for As, 4s for Na and 3d4s for Mn were treated as valence orbitals in the calculations. The projector augmented wave (PAW) potential [18] and the plane waves cut-off energy of 300 eV were used. For $CaZn_2As_2$ unit cell, a Γ-centered Monkhorst–Pack [19] k-point mesh of 5×5×3 was used and the internal atomic coordinates were relaxed until the force was less than 0.01 eV/Å. For Na and Mn co-doped $CaZn_2As_2$ supercell, a Γ-centered Monkhorst–Pack k-point mesh of

[1)]e-mail address: pjsd@163.com

1×3×3 was used. The criterion for the total energy was set as 10^{-4} eV.

3. Results and discussion. As a parent system, $CaZn_2As_2$ crystallizes in the hexagonal $CaAl_2Si_2$ structure with the space group $P\bar{3}m1$ (# 164), as shown in Fig. 1. The experimentally measured lattice constant of

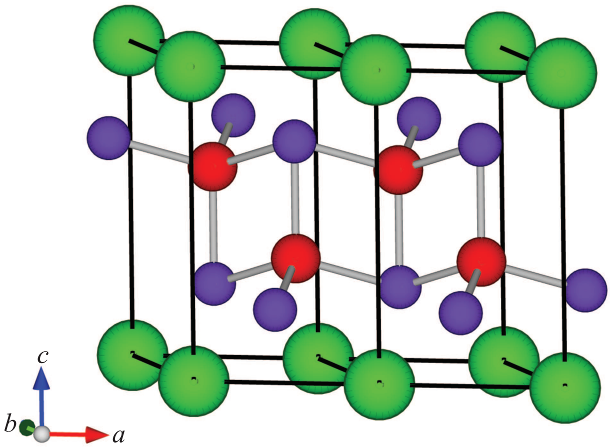

Fig. 1. (Color online) The crystal structure of the $CaZn_2As_2$, which is composed of a two unit cell. Green, red, and purple spheres represent Ca, Zn and As atoms, respectively

$CaZn_2As_2$ ($a = 4.162$ Å, $c = 7.010$ Å) [20] were used in our calculations and the internal coordinates were optimized. In Fig. 2 the density of states (DOS) of $CaZn_2As_2$

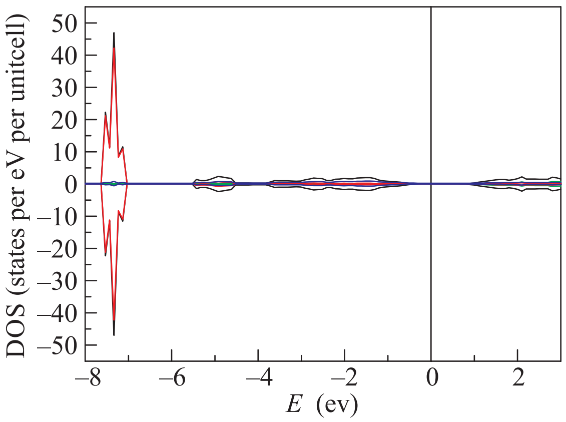

Fig. 2. (Color online) The total (black line) and partial density of states of Ca (green line), Zn (red line), and As (blue line) of $CaZn_2As_2$ per unitcell. The energy zero is taken at the Fermi level and indicated by the vertical line

is depicted. This compound is a non-magnetic semiconductor with a calculated band gap at about 0.7 eV, which is consistent with the previous theoretical report [21].

In order to gain insight into the properties of Na and Mn co-doped $CaZn_2As_2$, we first investigate the two Mn atom-doped $CaZn_2As_2$. We have used two Mn atoms to substitute two Zn atoms in a 5×2×1 supercell for constructing $Ca(Zn_{0.9}Mn_{0.1})_2As_2$. We have calculated eight kinds of configuration with Mn–Mn different distances. We found that energy difference between ferromagnetic (FM) and antiferromagnetic (AFM) state is less than 10 meV and negligible when Mn–Mn distance is larger than 7.21 Å. Thus, we have presented the five kinds of Mn–Mn pair configuration: (1) the first nearest neighboring two Mn atoms indicating *01*, (2) the second nearest neighboring two Mn atoms indicating *02*, (3) the third nearest neighboring two Mn atoms indicating *03*, (4) the fourth nearest neighboring two Mn atoms indicating *04*, (5) the fifth nearest neighboring two Mn atoms indicating *05*, as shown in Fig 3. Table 1 lists the energy of the $Ca(Zn_{0.9}Mn_{0.1})_2As_2$ FM and AFM state for the

Table 1. The total energy (eV) of the $Ca(Zn_{0.9}Mn_{0.1})_2As_2$ supercell with different configuration, magnetic moments (μ_B) of Mn atoms and distance (Å) between Mn–Mn pair configuration

	E_{FM}	E_{AFM}	ΔE	μ^{FM}/μ^{AFM}	distance
01	−183.3512	−183.5317	0.1805	4.30/4.26	3.018
02	−183.4464	−183.5172	0.0708	4.30/4.27	4.162
03	−183.4602	−183.4949	0.0347	4.29/4.28	5.143
04	−183.4715	−183.4836	0.0121	4.29/4.28	6.614
05	−183.4741	−183.4859	0.0118	4.30/4.28	7.208

five configurations. The energy difference ΔE between E_{FM} and E_{AFM} is defined as follows:

$$\Delta E = E_{FM} - E_{AFM}.$$

As observed from the Table 1, ΔE is positive for all five configurations and indicates the AFM is the ground state of $Ca(Zn_{0.9}Mn_{0.1})_2As_2$, which is consistent with the experiments [4]. In Fig. 4 we show the spin-polarized DOS of $Ca(Zn_{0.9}Mn_{0.1})_2As_2$ of *01* AFM configuration. We see that the contributions from the Mn 4s states to the valence bands of $Ca(Zn_{0.9}Mn_{0.1})_2As_2$ are negligible. So the Mn atoms are in the form of cation Mn^{2+}. The Mn1 (at 0 site) 3d major spin band are occupied and minor spin band empty while Mn2 (at 1 site) 3d spin band are reversed. There are no density of states at E_F. The electronic structure of Mn 3d states indicates the superexchange mechanism which leads to the antiferromagnetic coupling between the two Mn atoms [22]. In Mn atom-doped $CaZn_2As_2$, the As atoms around Mn atoms form an tetrahedral coordination ligand field, splitting d orbitals into e and t_2 states. The t_2 states of Mn hybridize with the ligand 4p orbitals of As, owing to the symmetry. The superexchange mechanism is

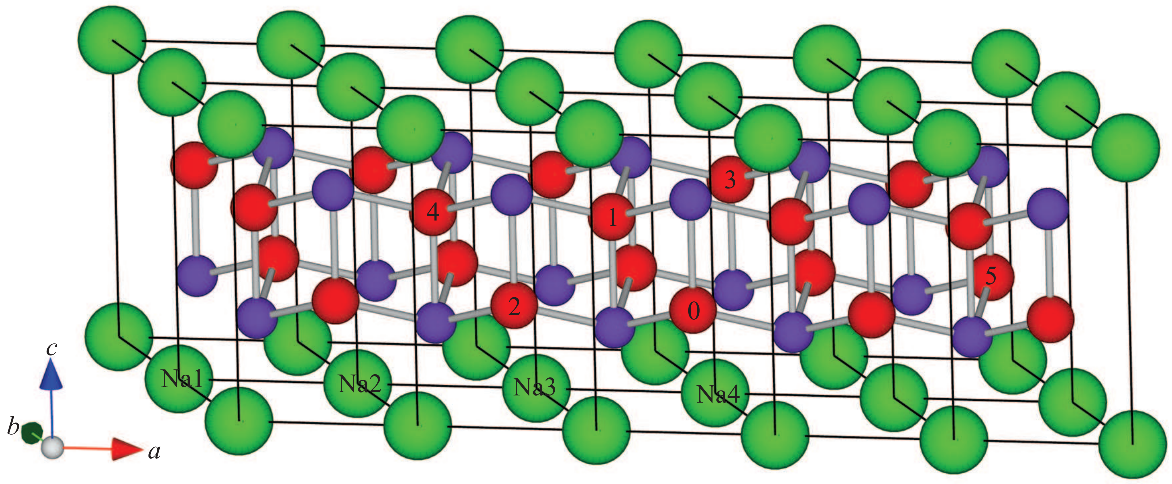

Fig. 3. (Color online) The 5×2×1 supercell of $CaZn_2As_2$. The configurations of Mn atom indicate *01*, *02*, *03*, *04*, *05* and the Na atom position Na1, Na2, Na3, Na4

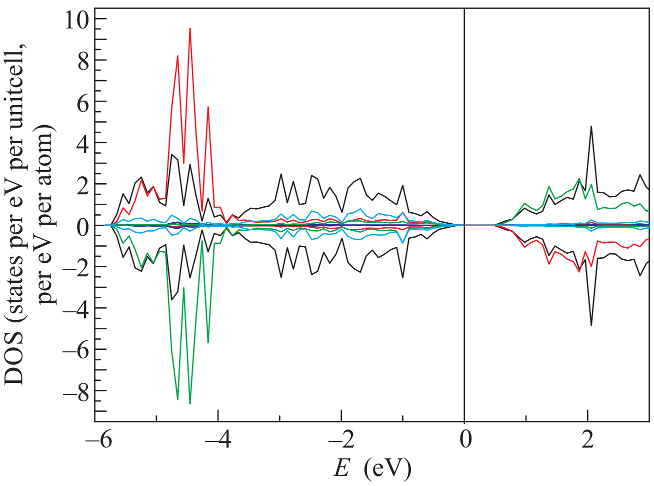

Fig. 4. (Color online) The total averaged (black line) and partial density of states of As 4p (cyan line) of $Ca(Zn_{0.9}Mn_{0.1})_2As_2$ per unit cell. The partial density of states of Mn1 3d (red line) 4s (blue line), Mn2 3d (green line) 4s (blue line) per atom. The energy zero is taken at the Fermi level and indicated by the vertical line

explained by magnetic coupling transferred by ligands, i.e., the p orbitals of the anions. As shown in Fig. 4, the filled 3d states of Mn are strongly hybridized with the As 4p states, giving a broad band with a width comparable to the As 4p states. Since the hybridization implies the intensity of chemical reaction and strong hybridization brings about a big solubility, the above results mean that the substituent concentration of Mn-doped $CaZn_2As_2$ will be high. This result is consistent with the substituent concentration of Mn-doped $CaZn_2As_2$ in experiment as high as 25 % [11]. From Fig. 4, we also see that the exchange splitting, due to the Mn 3d electrons localizing and onsite coulomb interaction, is larger than the crystal filed splitting. This leads to a high spin configuration of d^5 with the local magnetic moments of Mn atoms with $S = 5/2$, which is consistent with our calculated moment. From Table 1, we also note that ΔE decreases quickly with the increasing distance between Mn–Mn pairs, which means that the Mn–Mn antiferromagnetic interaction comes from short range superexchange mechanism.

Table 2. The calculated energy (eV) of the different positions of Na atom of ferromagnetic and antiferromagnetic states of $(Ca_{0.9}Na_{0.1})(Zn_{0.9}Mn_{0.1})_2As_2$

Na position		E_{FM}	E_{AFM}	ΔE
Na1	01	−181.0391	−181.1944	0.1553
	02	−181.1438	−181.1793	0.0355
	03	−181.1539	−181.1602	0.0063
	04	−181.1614	−181.1549	−0.0065
	05	−181.1803	−181.1746	-0.0057
Na2	01	−181.0500	−181.1949	0.1449
	02	−181.1250	−181.1418	0.0168
	03	−181.1539	−181.1601	0.0062
	04	−181.1847	−181.1695	−0.0152
	05	−181.1620	−181.1594	−0.0026
Na3	01	−181.0517	−181.1600	0.1083
	02	−181.1526	−181.1523	−0.0003
	03	−181.1129	−181.1058	−0.0071
	04	−181.1583	−181.1464	−0.0119
	05	−181.1326	−181.1284	−0.0042
Na4	01	−181.0993	−181.2100	0.1107
	02	−181.1633	−181.1644	0.0011
	03	−181.2101	−181.1920	−0.0181
	04	−181.1858	−181.1706	−0.0152
	05	−181.1813	−181.1793	−0.0020

Secondly, with the same supercell, we have replaced one Ca atom with a Na atom to construct $(Ca_{0.9}Na_{0.1})(Zn_{0.9}Mn_{0.1})_2As_2$. In terms of different distances between Mn atoms and Na atoms, we introduce four kinds of Na atoms named Na1, Na2, Na3, Na4 as shown in Fig. 3. Table 2 lists the energy of different Na positions of FM and AFM states of $(Ca_{0.9}Na_{0.1})(Zn_{0.9}Mn_{0.1})_2As_2$. For Mn–Mn nearest neighboring configuration *01*, the AFM state between Mn atoms is stable regardless of the position of Na atoms. This result verifies the surmise in reference 11 that Mn moments are antiferromagnetic coupled in the nearest neighbor Zn sites. With the Mn–Mn distance increasing, the coupling of Mn–Mn atoms changes from AFM to FM for all Na substitution. This means that there is a competition between AFM and FM coupling in the $(Ca_{0.9}Na_{0.1})(Zn_{0.9}Mn_{0.1})_2As_2$. The Mn–Mn antiferromagnetic interaction is very strong and short ranged, which play a major role in the first nearest neighbor Mn–Mn configuration. The ferromagnetic interaction is relatively weak but longer ranged. When the Mn–Mn distance is larger than the third nearest neighbor, the FM interaction overtakes AFM interaction. For 10 % of Mn substitution, the average distance between Mn ions is about 6.619 Å which approximate the fourth nearest neighbor (6.614 Å). This means that the FM coupling of Mn atoms should be ground state in the real alloy where the Mn ions are randomly distributed.

To elucidate the origin of ferromagnetic coupling between Mn atoms, we have calculated the density of states of $(Ca_{0.9}Na_{0.1})(Zn_{0.9}Mn_{0.1})_2As_2$ of Na4 position of Mn *03* FM configuration and shown in Fig. 5. From Fig. 5 we see that the contributions from the Na 4s states to the valence bands of $(Ca_{0.9}Na_{0.1})(Zn_{0.9}Mn_{0.1})_2As_2$ are negligible. This means that the Na atom is in the form of cation Na^{1+}. The DOS in Fig. 5 shows the semimetallic behavior for the compound. The hole carriers are introduced into the empty states near the Fermi level, which is mostly composed of the As 4p states. So the delocalized holes have a character of the host states near the top of the valence band with a small admixture of the Mn 3d orbital weight. At the same time, the main peak in the partial density of states of the majority spin Mn $3d^5$ electrons is well below the Fermi level and these states form a local moment. Thus, the ferromagnetic coupling between Mn local moments is mediated by delocalized band holes via Zener's p-d exchange interaction [22].

4. Summary. In conclusion, we have performed a study of the electronic structure and magnetic properties of Na and Mn co-doped $CaZn_2As_2$ using density functional theory within the GGA+U schemes. We

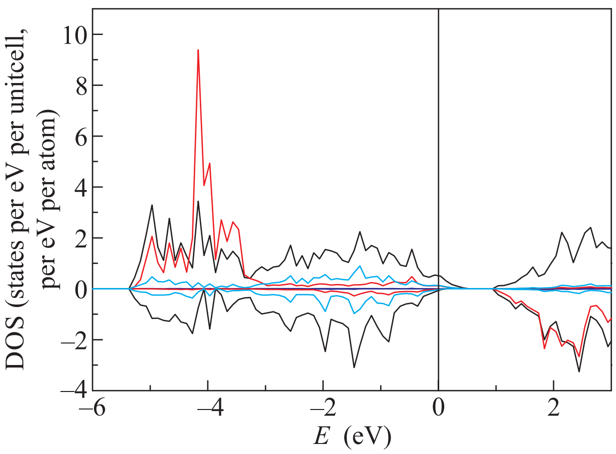

Fig. 5. (Color online) The total averaged (black line) and partial density of states of As 4p (cyan line) of $(Ca_{0.9}Na_{0.1})(Zn_{0.9}Mn_{0.1})_2As_2$ per unit cell. The partial density of states of Na 4s (blue line) and Mn 3d (red line) per atom. The energy zero is taken at the Fermi level and indicated by the vertical line

have shown that the superexchange mechanism leads to the antiferromagnetic coupling between Mn atoms in Mn-doped $CaZn_2As_2$. The ferromagnetic origin of Na and Mn co-doped $CaZn_2As_2$ is hole carriers mediated via Zener's p-d exchange interaction.

1. H. Ohno, Science **281**, 951 (1998).
2. T. Dietl, Nat. Mater. **9**, 965 (2010).
3. T. Dietl, H. Ohno, F. Matsukura, J. Cibert, and D. Ferrand, Science **287**, 1019 (2000).
4. Z. Deng, C. Q. Jin, Q. Q. Liu et al. (Collaboration), Nat. Commun. **2**, 041102R (2013).
5. Z. Deng, K. Zhao, B. Gu et al. (Collaboration), Phys. Rev. B **88**, 081203(R) (2013).
6. C. Ding, H. Man, C. Qin et al. (Collaboration), Phys. Rev. B **88**, 041102R (2013).
7. W. Han, K. Zhao, X. C. Wang, Q. Q. Liu, F. L. Ning, Z. Deng, Y. Liu, C. Ding, and C. Q. Jin, Sci. China. Phys. Mech. Astron. **56**, 2026 (2013).
8. X. J. Yang, Y. K. Li, C. Y. Shen, B. Q. Si, Y. L. Sun, Q. Tao, C. Cao, Z. A. Xu, and F. C. Zhang, Appl. Phys. Lett. **103**, 022410 (2013).
9. K. Zhao, Z. Deng, X. C. Wang et al. (Collaboration), Nat. Commun. **4**, 1422 (2013).
10. K. Zhao, B. J. Chen, G. Q. Zhao, Z. Yuan, Q. Q. Liu, Z. Deng, J. L. Zhu, and C. Q. Jin, Chin. Sci. Bull. **59**, 2524 (2014).
11. K. Zhao, B. J. Chen, Z. Deng et al. (Collaboration), J. Appl. Phys. **116**, 163906 (2014).
12. B. J. Chen, K. Zhao, Z. Deng et al. (Collaboration), Phys. Rev. B. **90**, 155202 (2014).

13. J. P. Perdew, K. Burke, and M. Ernzerhof, Phys. Rev. Lett. **77**, 3865 (1996).
14. G. Kresse and J. Furthmüller, Phys. Rev. B **54**, 11169 (1996).
15. A. I. Liechtenstein, V. I. Anisimov, and J. Zaanen, Phys. Rev. B **52**, R5467 (1995).
16. J. Okabayashi, A. Kimura, O. Rader, T. Mizokawa, A. Fujimori, T. Hayashi, and M. Tanaka, Phys. Rev. B **58**, 4211 (1998).
17. K. Sato, P. H. Dederichs, H. Katayama, and J. Kudrnovsky, J. Phys.: Condens. Matter. **16**, 5491 (2004).
18. P. E. Blöchl, Phys. Rev. B **50**, 17953 (1994).
19. H. J. Monkhorst and J. D. Pack, Phys. Rev. B **13**, 5188 (1976).
20. P. Klüfers and A. Mewis, Z. Naturforsch **32b**, 753 (1977).
21. F. Wartenberga, C. Kranenberga, R. Pochaa, D. Johrendta, A. Mewisa, R. D. Hoffmannb, B. D. Moselc, and R. Pöttgenb, Z. Naturforsch **57b**, 1270 (2002).
22. K. Sato, L. Bergqvist, J. Kudrnovsky, P. H. Dederichs, O. Eriksson, I. Turek, B. Sanyal, G. Bouzerar, H. Katayama-Yoshida, V. A. Dinh, T. Fukushima, H. Kizaki, and R. Zeller, Rev. Mod. Phys. **82**, 1633 (2010).